Targeted energy transfer under harmonic forcing with a vibro-impact nonlinear energy sink: analytical and experimental developments

Etienne Gourc, Guilhem Michon, Sébastien Seguy, Alain Berlioz

Targeted energy transfer under harmonic forcing with a vibro-impact nonlinear energy sink : analytical and experimental developments

Etienne Gourc

Université de Toulouse

Institut Clément Ader, INSA

F-31077, Toulouse, France

Guilhem Michon

Université de Toulouse

Institut Clément Ader, ISAE

F-31055, Toulouse, France

Sébastien Seguy

Université de Toulouse

Institut Clément Ader, INSA

F-31077, Toulouse, France

Alain Berlioz

Université de Toulouse

Institut Clément Ader, UPS

F-31062, Toulouse, France

ABSTRACT

Recently, it has been demonstrated that a vibro-impact type nonlinear energy sink (VI-NES) can be used ef-

ficiently to mitigate vibration of a linear oscillator (LO) under transient loading. The objective of this paper is to investigate theoretically and experimentally the potential of a VI-NES to mitigate vibrations of a LO subjected to a harmonic excitation (nevertheless, the presentation of an optimal VI-NES is beyond the scope of this paper). Due to the small mass ratio between the LO and the flying mass of the NES, the obtained equation of motion are analyzed using the method of multiple scales in the case of $1:1$ resonance. It is shown that in addition to periodic response, system with VI-NES can exhibit strongly modulated response (SMR). Experimentally, the whole system is embedded on an electrodynamic shaker. The VI-NES is realized with a ball which is free to move in a cavity with a predesigned gap. The mass of the ball is less than 1% of the mass of the LO. The experiment confirms the existence of periodic and SMR response regimes. A good agreement between theoretical and experimental results is observed.

Introduction

Targeted energy transfer (TET), also called energy pumping has been widely studied during the last decade. In this context, a small mass, strongly nonlinear oscillator called a NES is used to mitigate any unwanted disturbance introduced in a primary system (i.e. LO) by efficiently transferring and eliminating energy from the main system to the NES.

Energy pumping under transient loading has been extensively studied. In [1, 2], it has been shown that the main phenomena allowing TET is based on the $1:1$ resonance capture. Experimental verifications are presented in [3–5].

TET under external forcing has also been studied. Introduction of a suitable asymptotic procedure based on the invariant manifold approach [6] has shown that in addition to periodic regimes, system with NES can exhibit beating response, referred as strongly modulated response (SMR) [7]. This type of response has been verified experimentally in [8]. The use of NES to passively control instability is also a growing interest. In [9], a NES is used to control limit cycle oscillation of a Van der Pol system. [10–13] studied the effectiveness of a NES to suppress aeroelastic instability. In [14], it is shown that a NES can be used to control chatter instability in turning.

All the aforementioned studies deal with NES with cubic non-linearity. Recent studies have enlighten that non-smooth system can be used as NES. One of the main advantage of this type of NES over classic NES is that they are often easier to build than classic NES. Gendelman investigated energy transfer in system with non-polynomial nonlinearity [15]. NES with piecewise linear stiffness have been studied in [16] under transient and periodic forcing. The case of a vertical NES, considering its own weight has been reported in [17].

Vibro-impact type NES (VI-NES) have been studied in [18–20]. However, these study were concentrated around numerical simulations. In a recent study, the invariant manifold approach has been extended to VI-NES under transient loading [21].

In this paper an harmonically forced linear oscillator (LO) with an embedded VI-NES is considered theoretically, using the invariant manifold approach and experimentally. The behavior of the system is studied in the regime of $1:1$ resonance. The structure of the paper is as follow. Section 2, is devoted to the analytic treatment of the governing equation of motion. In section 3, analytic results are presented and are compared to numerical simulation. In the next section, the experimental setup is presented. Measurements are compared to analytical and numerical results. Finally, concluding remarks are addressed.

1 Theoretical developments

The system considered is composed of a linear oscillator (LO) with an embedded vibro-impact nonlinear energy sink (VI-NES). The LO is subjected to an imposed base displacement. The system is presented in Fig. 1. The reduced governing equation of motion, between impact, are expressed as:

$$\begin{gathered}\ddot{x}_1+\varepsilon\lambda\dot{x}_1+x_1=\varepsilon A\sin\Omega t+\varepsilon^2\lambda A\Omega\cos\Omega t\\ \ddot{x}_2=0,\quad \forall|x_1-x_2|<\Delta\end{gathered}\tag{1}$$

The corresponding physical parameters are expressed as:

$$\begin{gathered}\varepsilon=\frac{m_2}{m_1},\quad \omega_1^2=\frac{k_1}{m_1},\quad \lambda=\frac{c_1}{m_2\omega_1},\\ A=\frac{G}{\varepsilon},\quad \Omega=\frac{\omega}{\omega_1},\quad t=\omega_1\tilde{t}\end{gathered}$$

where x_1 and x_2 are the displacement of the LO and the NES respectively and the dots denotes differentiation with respect to the non-dimensional time t. The excitation amplitude G has been scaled to order ε to appear as the same order as damping.

[Fig. 1 about here.]

When $|x_1-x_2|=\Delta$, a collision occurs. The state of the system after impact is obtained using the simplified shock theory and the condition of total momentum conservation:

$$\begin{gathered}x_1^+=x_1^-,\quad x_2^+=x_2^-\\ \dot{x}_1^++\varepsilon\dot{x}_2^+=\dot{x}_1^-+\varepsilon\dot{x}_2^-,\quad \dot{x}_1^+-\dot{x}_2^+=-r\left(\dot{x}_1^--\dot{x}_2^-\right),\\ \text{for } |x_1-x_2|=\Delta\end{gathered}\tag{2}$$

where r is the restitution coefficient of impact and the superscripts $+$ and $-$ denotes time immediately after and before impact. New variables representing the displacement of the center of mass and the internal displacement of the VI-NES are introduced as follow:

$$v=x_1+\varepsilon x_2,\quad w=x_1-x_2\tag{3}$$

Substituting Eq. (3) into Eqs. (1) and (2), the equation between impact in barycentric coordinate are given as:

$$\begin{gathered}\ddot{v}+\varepsilon\lambda\frac{\dot{v}+\varepsilon\dot{w}}{1+\varepsilon}+\frac{v+\varepsilon w}{1+\varepsilon}=\varepsilon A\sin\Omega t+\varepsilon^2\lambda A\Omega\cos\Omega t\\ \ddot{w}+\varepsilon\lambda\frac{\dot{v}+\varepsilon\dot{w}}{1+\varepsilon}+\frac{v+\varepsilon w}{1+\varepsilon}=\varepsilon A\sin\Omega t+\varepsilon^2\lambda A\Omega\cos\Omega t\\ \forall|w|<\Delta\end{gathered} \tag{4}$$

and the impact condition (2) is rewritten as:

$$\begin{gathered}v^+=v^-,\quad w^+=w^-,\\ \dot{v}^+=\dot{v}^-,\quad \dot{w}^+=-r\dot{w}^-,\quad \text{for } |w|=\Delta\end{gathered} \tag{5}$$

In the context of energy pumping, the mass ratio ε is supposed to be small ($\approx 1\%$). In this case, Eq. (4) may be analyzed by multiple scales approach with respect to this small parameter. Multiple scales are introduced in the form:

$$\begin{gathered}v(t;\varepsilon)=v_0(T_0,T_1)+\varepsilon v_1(T_0,T_1)+\ldots,\\ w(t;\varepsilon)=w_0(T_0,T_1)+\varepsilon w_1(T_0,T_1)+\ldots\\ T_k=\varepsilon^k t,\quad k=0,1,\ldots\end{gathered} \tag{6}$$

We are interested in the behavior of the system in the vicinity of the $1:1$ resonance where the LO oscillates with a frequency close to external forcing while the VI-NES operates with two symmetric impact per cycle. A detuning parameter (σ) representing the nearness of the excitation frequency Ω to the reduced natural frequency of the LO is introduced:

$$\Omega=1+\varepsilon\sigma \tag{7}$$

Substituting Eqs. (6) and (7) into Eqs. (4), (5) and equating coefficients of like power of ε gives:

Order ε^0:

$$\begin{aligned} D_0^2 v_0 + v_0 &= 0 \\ D_0^2 w_0 + v_0 &= 0, \quad \forall |w_0| < \Delta \end{aligned} \tag{8}$$

$$\begin{aligned} v_0^+ &= v_0^-, \quad w_0^+ = w_0^-, \\ D_0 v_0^+ &= D_0 v_0^-, \quad D_0 w_0^+ = -r D_0 w_0^-, \quad \text{for } |w_0| = \Delta \end{aligned} \tag{9}$$

Order ε^1:

$$D_0^2 v_1 + v_1 = -2 D_0 D_1 v_0 - \lambda D_0 v_0 - w_0 + v_0 + A \sin(T_0 + \sigma T_1) \tag{10}$$

where $D_i^j = \partial^j / \partial T_i^j$. Analytic treatment of $O(\varepsilon^0)$ equation is based on [21]. The first equation of system (8), taking into account Eq. (9) simply represents an undamped harmonic oscillator and its solution can be expressed as follow:

$$v_0 = C(T_1) \sin(T_0 + \theta(T_1)) \tag{11}$$

The second equation of system (8) with (9) represents a harmonically forced impact oscillator with symmetric barrier. Under the assumption of $1:1$ resonance and motion with two symmetric impact per cycle, its solution can be searched in the following form [21]:

$$w_0 = C(T_1) \sin(T_0 + \theta(T_1)) + \frac{2}{\pi} B(T_1) \Pi(T_0 + \eta(T_1)) \tag{12}$$

where $\Pi(z)$ is a non-smooth zig-zag function. This folded function and its derivative is depicted in Fig. 2 and are expressed as follow:

[Fig. 2 about here.]

$$\Pi(z) = \arcsin(\sin z), \quad M(z) = \frac{d\Pi}{dz} = sgn(\cos z) \tag{13}$$

According to Eq. (12) and (13), impact occurs at $T_0 = \pi/2 - \eta + j\pi$ with $j = 0, 1, 2, \ldots$. The impact condition $|w_0| = \Delta$ is rewritten with Eq. (12) as:

$$C\cos(\eta - \theta) = \Delta - B \tag{14}$$

Rewriting now the inelastic impact condition (9) yields:

$$C(1+r)\sin(\eta - \theta) = \frac{2}{\pi}B(1-r) \tag{15}$$

Combining Eqs. (14) and (15), a relation between the slow variables B and C is obtained as follow:

$$C^2 = \left(1 + \frac{4(1-r)^2}{\pi^2(1+r)^2}\right)B^2 - 2\Delta B + \Delta^2 \tag{16}$$

As it has been reported in [21], Eq. (16) defines the expression of the slow invariant manifold (SIM) of the problem in the case of $1:1$ resonance. An example of SIM is depicted in Fig. 3 for $\Delta = 0.015$ and $r = 0.65$. Note that the value of r is a realistic value for the restitution coefficient in the case of steel-steel contact. As seen on Fig. 3, the SIM is divided in two branches. The stability of the SIM is evaluated by direct numerical integration of Eq. (9). The left part of the SIM is unstable, while a part of the right side is stable. As depicted on the phase space in Fig. 3, the $1:1$ motion with two symmetric impact per cycle is stable until $B \approx 0.0255$. For higher values of B, the motion becomes asymmetric, then $1:1$ symmetric motion is referred as unstable. Further increase of B can degenerate into motion with more than two impact per cycle. The extrema of the SIM is computed by equating the derivative of the right hand side of Eq. (16) to zero:

$$
\begin{aligned}
B_1 &= \frac{\Delta\pi^2\left(1+r\right)}{\pi^2\left(1+r\right)+4\left(1-r\right)} \\
C_1^2 &= \frac{4\Delta^2\left(1-r\right)^2}{\pi^2\left(1+r\right)^2+4\left(1-r\right)^2}
\end{aligned}
\tag{17}
$$

[Fig. 3 about here.]

The value C_1 corresponds to the minimum amplitude of the LO which allow 1 : 1 TET.

The influence of the topology of the SIM as well as the process of TET may be verified by analyzing the dynamic of system (1) under transient loading. In Fig. 4, the result of numerical integration of the equation of motion under transient loading ($\dot{u}(0) \neq 0$) is depicted. The phase difference $\eta - \theta$ as well as the projection of the numerical integration on the SIM are presented.

[Fig. 4 about here.]

Rapid decay of the main system is observed and the resonance capture is confirmed by looking at the phase difference between the VI-NES and the LO. Effectively, during resonance capture, the phase difference exhibit a non time-dependent behavior. When the amplitude of the system decay until reaching the minimal value of the SIM C_1, the system escape from resonance capture an the VI-NES perform chaotic-like motion. This scenario is analog to the one observed for NES with cubic stiffness coupling and confirm the potential of using a VI-NES under transient loading.

In order to study the dynamics of the system under harmonic forcing, Eq. (10) at the next order of approximation is analyzed. To identify terms that produce secular terms, the function $\Pi(z)$ in Eq. (13) is expanded in Fourier series:

$$
\Pi(z) = \sum_{k=1}^{\infty} \frac{-4\left(-1\right)^k}{\pi\left(2k-1\right)^2} \sin\left(\left(2k-1\right)t\right) \tag{18}
$$

Substituting Eq. (11), (12) and (18) into Eq. (10) and eliminating terms that produce secular terms gives:

$$
\begin{aligned}
-2D_1 C\cos\theta + 2C\sin\theta D_1\theta - \lambda C\cos\theta \\
-\frac{8}{\pi^2}B\sin\eta + A\sin(\sigma T_1) = 0 \\
2D_1 C\sin\theta + 2C\cos\theta D_1\theta + \lambda C\sin\theta \\
-\frac{8}{\pi^2}B\cos\eta + A\cos(\sigma T_1) = 0
\end{aligned}
\tag{19}
$$

Rearranging in a more convenient form yields:

$$\begin{aligned} 2CD_1\theta &= \frac{8}{\pi^2}B\cos(\eta-\theta) - A\cos(\sigma T_1-\theta) \\ 2D_1C &= -\lambda C - \frac{8}{\pi^2}B\sin(\eta-\theta) + A\sin(\sigma T_1-\theta) \end{aligned} \tag{20}$$

Substituting Eqs. (14), (15) into Eq. (20) and introducing $\gamma = \sigma T_1 - \theta$, the following equations are obtained:

$$\begin{aligned} 2CD_1\gamma &= -\frac{8B(\Delta-B)}{\pi^2 C} + A\cos\gamma + 2C\sigma \\ 2D_1C &= -\frac{16B^2(1-r)}{\pi^3 C(1+R)} + A\sin\gamma - \lambda C \end{aligned} \tag{21}$$

The fixed points are computed by equating the derivative of the right hand side of Eq. (21) to zero:

$$\begin{aligned} -\frac{8B}{C\pi^2}(\Delta-B) + A\cos\gamma + 2C\sigma &= 0 \\ -\frac{16B^2(1-r)}{\pi^3 C(1+R)} + A\sin\gamma - \lambda C &= 0 \end{aligned} \tag{22}$$

Using trigonometric identities and solving for C^2, new relations between C and B are obtained:

$$C^2 = b_1 B, \quad C^2 = b_2 B \tag{23}$$

Finally, the fixed points of the slow-flow can be obtained graphically as the intersection of the SIM (16), and the curve b_1 and/or b_2. Fixed points can also been expressed by equating the right hand sides of Eq. (16) and Eq. (23). A fourth order polynomial in B is then obtained. The stability of the fixed points has not been analyzed herein and will be studied in future developments.

2 Numerical simulations

In this section, various response regimes for different values of parameters are presented. Numerical simulations highlights the relation between the topology of the SIM, and the global behavior of the system.

In Fig. 5, the SIM (16), denoted by blue line, and the curves (23), denoted by green lines are presented for the following set of parameters:

$$\begin{aligned} \varepsilon = 0.84\%, \quad \lambda = 0.95, \quad A = 0.015, \\ \Delta = 0.015, \quad r = 0.65, \quad \sigma = -0.2 \end{aligned} \tag{24}$$

At their intersection, red circle (o) and cross (+) represents stable and unstable fixed points respectively. In the present case, the green curves intersect the SIM two times. The fixed point located on the left side of the SIM is unstable, while the one located on the right branch of the SIM is stable.

[Fig. 5 about here.]

If the initial condition are in the domain of attraction of the SIM, the flow will be automatically attracted to the stable fixed points. The system will exhibit periodic motion with two symmetric impact per cycle. This prediction is confirmed by numerical integration of system (4), (5) depicted in Fig. 6. The displacement of the center of mass (v) for parameters (24) is presented. As expected from Fig. 5, after a short transient, the flow is rapidly attracted to the fixed points and stable periodic response is observed.

[Fig. 6 about here.]

Another set of parameters where stable fixed points does not exist is now considered:

$$\begin{aligned} \varepsilon = 0.84\%, \quad \lambda = 0.95, \quad A = 0.012, \\ \Delta = 0.015, \quad r = 0.65, \quad \sigma = 0 \end{aligned} \tag{25}$$

The diagram of the slow-flow on the SIM is presented in Fig. 7 for the set of parameters (25). In this case two unstable fixed points are located on the lower branch of the SIM. The only possible response for the system is stable strongly modulated response (SMR). This regime is observed on the numerical integration at Fig. 8. Contrary to NES with cubic stiffness [7, 22], where, during SMR, the flow jumps between two stable branches, in this case, it is observed that SMR act through successive synchronization between the LO and the VI-NES. When the VI-NES is not synchronized, the amplitude of the LO grows, under certain circumstance, the VI-NES enter in a $1:1$ resonance capture with the LO. Then energy in the system is dissipated by successive impacts and the amplitude of the LO decays until $C = C_1$ (17). Finally, the NES escapes resonance capture, and the amplitude of the LO starts growing again. Such a behavior can not be explained by only studying the fixed points of the system.

[Fig. 7 about here.]

[Fig. 8 about here.]

3 Experimental trials

The experimental setup is depicted in Fig. 9(a). It consists of a LO, with an embedded VI-NES. The whole system is embedded on $10kN$ electrodynamic shaker. The displacement of the LO as well as the imposed displacement of the shaker are measured using contact-less laser displacement sensors. A detailed view of the VI-NES is presented in Fig. 9(b). It simply consists of a closed cavity of length $d+2\Delta$, where d is the diameter of the ball. Each cover is made of hardened steel. The design of the VI-NES is voluntary simple to check whether this kind of system can be used as vibration mitigation device. Note that the aim of this experiment is not to built an efficient NES, but to investigate the different response regimes for future exploration.

The parameters of the system have been identified by performing modal analysis and are summarized in Table 1.

[Fig. 9 about here.]

[Table 1 about here.]

Experimental trials have been carried out for three different forcing amplitudes. For each trial, displacement of the LO has been recorded for increasing and decreasing frequency around the natural frequency of the LO. The first results for $G = 0.16mm$ ($A = 0.019$) is depicted in Fig. 10. Blue lines are the analytical fixed points. Red dashed vertical lines represent the zone of SMR found using numerical integration of Eqs. (3), (4). Green lines represents measured periodic response and straight vertical lines represents the experimentally determined zone of SMR. First periodic response were observed for $\sigma = -3.2$. This branch of periodic solution has been followed until $\sigma = 1.1$. For further increase of the forcing frequency, periodic solution loose its stability, and SMR response takes place as illustrated in Fig. 4.

[Fig. 10 about here.]

[Fig. 11 about here.]

Experimentally, it has been found that stable SMR takes place between $\sigma = 1.25$ and $\sigma = 2.22$ versus $\sigma = 1.6$ and $\sigma = 3$ numerically. Similar results are obtained for a reduced forcing amplitude ($G = 0.14mm$, $A = 0.017$) and are depicted in Fig. 12. In this case, periodic motion is still observed between $\sigma = -2.08$ and $\sigma = 0.42$. SMR response is also observed between $\sigma = 0.55$ and $\sigma = 1.8$ experimentally versus $\sigma = 0.9$ and $\sigma = 2.6$ numerically.

[Fig. 12 about here.]

Decreasing the forcing amplitude to $G = 0.125mm$ ($A = 0.015$), the behavior of the system changes drastically and is presented in Fig. 13. For this case, a stable fixed does not exist, and SMR regimes are observed for a larger zone of forcing frequency. Experimentally, SMR has been observed from $\sigma = -1.94$ to $\sigma = 1.39$, versus $\sigma = -2.2$ and $\sigma = 2.4$ numerically.

[Fig. 13 about here.]

This last trial is of particular interest since high amplitude fixed points are not observed anymore, and passive control through SMR occurs on a larger bandwidth. Despite the small mass ratio between the mass of the ball and the mass of the LO, the VI-NES strongly influences the global behavior of the system. Qualitative behavior is explained theoretically, and correspondence between analytical/numerical and experimental results is observed.

4 Conclusion

In this paper, the dynamic response of a two dof system comprising a linear oscillator, subjected to an imposed harmonic displacement, with an embedded vibro-impact nonlinear energy sink (VI-NES) is investigated theoretically and experimentally. The VI-NES consist of a ball free to move inside rigid barrier. The collision is modeled using simplified shock theory, and a realistic restitution coefficient is taken into account. Equation of motion around the $1:1$ resonance are analyzed using a multiple scales approach. Symmetric motion with two symmetric impact per cycle are considered. The existence of periodic solution as well as SMR is explained. An experimental device is built. Measurements of frequency response curve for three different forcing amplitudes are presented and compared to analytical predictions. Periodic regimes and also SMR response are observed. The experimentally determined SMR zone is compared to numerical simulation. Even if the model of the NES is a rough approximation of the real motion of the ball, a good agreement between theoretical and experimental results is observed. The correspondence between theoretical and experimental results may be improved by considering a more realistic model of impact and friction inside the cylinder, especially for low speed impact and low amplitude excitation. This type of NES is easy to realize and could be easily integrated in real structure. These results are encouraging to deeper investigate the behavior of this type of NES.

References

[1] Gendelman, O., Manevitch, L., Vakakis, A., and M'Closkey, R., 2001. "Energy pumping in nonlinear mechanical oscillators: Part i: Dynamics of the underlying hamiltonian systems". *Journal of Applied Mechanics,* ***68***(1), pp. 34–41.

[2] Vakakis, A., and Gendelman, O., 2001. "Energy pumping in nonlinear mechanical oscillators: Part ii: Resonance capture". *Journal of Applied Mechanics,* ***68***(1), pp. 42–48.

[3] McFarland, D., Bergman, L., and Vakakis, A., 2005. "Experimental study of non-linear energy pumping occurring at a single fast frequency". *International Journal of Non-Linear Mechanics,* ***40***(6), pp. 891–899.

[4] Gourdon, E., Alexander, N., Taylor, C., Lamarque, C., and Pernot, S., 2007. "Nonlinear energy pumping under transient forcing with strongly nonlinear coupling: Theoretical and experimental results". *Journal of Sound and Vibration,* ***300***(3), pp. 522–551.

[5] Kerschen, G., Kowtko, J., McFarland, D., Bergman, L., and Vakakis, A., 2007. "Theoretical and experimental study of multimodal targeted energy transfer in a system of coupled oscillators". *Nonlinear Dynamics,* ***47***(1), pp. 285–309.

[6] Gendelman, O., 2004. "Bifurcations of nonlinear normal modes of linear oscillator with strongly nonlinear damped attachment". *Nonlinear Dynamics,* ***37***(2), pp. 115–128.

[7] Starosvetsky, Y., and Gendelman, O., 2008. "Strongly modulated response in forced 2dof oscillatory system with essential mass and potential asymmetry". *Physica D: Nonlinear Phenomena,* ***237***(13), pp. 1719–1733.

[8] Gourc, E., Michon, G., Seguy, S., and Berlioz, A., 2013. "Experimental investigation and design optimization of targeted energy transfer under periodic forcing". *Journal of Vibration and Acoustics,* ***136***.

[9] Gendelman, O., and Bar, T., 2010. "Bifurcations of self-excitation regimes in a van der pol oscillator with a nonlinear energy sink". *Physica D: Nonlinear Phenomena,* ***239***(3), pp. 220–229.

[10] Lee, Y., Vakakis, A., Bergman, L., McFarland, D., and Kerschen, G., 2007. "Suppressing aeroelastic instability using broadband passive targeted energy transfers, part 1: Theory". *AIAA journal,* ***45***(3), pp. 693–711.

[11] Lee, Y., Kerschen, G., McFarland, D., Joel Hill, W., Nichkawde, C., Strganac, T., Bergman, L., and Vakakis, A., 2007. "Suppressing aeroelastic instability using broadband passive targeted energy transfers, part 2: experiments". *AIAA journal,* ***45***(10), pp. 2391–2400.

[12] Gendelman, O., Vakakis, A., Bergman, L., and McFarland, D., 2010. "Asymptotic analysis of passive nonlinear suppression of aeroelastic instabilities of a rigid wing in subsonic flow". *SIAM Journal on Applied Mathematics,* ***70***(5), pp. 1655–1677.

[13] Vaurigaud, B., Manevitch, L., and Lamarque, C., 2011. "Passive control of aeroelastic instability in a long span bridge model prone to coupled flutter using targeted energy transfer". *Journal of Sound and Vibration,* ***330***(11), pp. 2580–2595.

[14] Gourc, E., Seguy, S., Michon, G., and Berlioz, A., 2013. "Chatter control in turning process with a nonlinear energy sink". *Advanced Materials Research,* ***698***, pp. 89–98.

[15] Gendelman, O., 2008. "Targeted energy transfer in systems with non-polynomial nonlinearity". *Journal of Sound and Vibration,* ***315***(3), pp. 732–745.

[16] Lamarque, C., Gendelman, O., Ture Savadkoohi, A., and Etcheverria, E., 2011. "Targeted energy transfer in mechanical systems by means of non-smooth nonlinear energy sink". *Acta mechanica,* ***221***(1), pp. 175–200.

[17] Ture Savadkoohi, A., Lamarque, C., and Dimitrijevic, Z., 2012. "Vibratory energy exchange between a linear and a nonsmooth system in the presence of the gravity". *Nonlinear Dynamics,* ***70***, pp. 1–11.

[18] Nucera, F., Vakakis, A., McFarland, D., Bergman, L., and Kerschen, G., 2007. "Targeted energy transfers in vibro-impact oscillators for seismic mitigation". *Nonlinear Dynamics,* ***50***(3), pp. 651–677.

[19] Nucera, F., Lo Iacono, F., McFarland, D., Bergman, L., and Vakakis, A., 2008. "Application of broadband nonlinear targeted energy transfers for seismic mitigation of a shear frame: Experimental results". *Journal of Sound and Vibration,* ***313***(1), pp. 57–76.

[20] Lee, Y., Nucera, F., Vakakis, A., McFarland, D., and Bergman, L., 2009. "Periodic orbits, damped transitions and targeted energy transfers in oscillators with vibro-impact attachments". *Physica D: Nonlinear Phenomena,* ***238***(18), pp. 1868–1896.

[21] Gendelman, O., 2012. "Analytic treatment of a system with a vibro-impact nonlinear energy sink". *Journal of Sound and Vibration,* ***331***, p. 45994608.

[22] Gourc, E., Seguy, S., Michon, G., and Berlioz, A., 2012. "Delayed dynamical sytem strongly coupled to a nonlinear energy sink: application to machining chatter". In MATEC Web of Conferences, Vol. 1, EDP Sciences.

List of Tables

List of Figures

Table 1. Parameters of the experiment

Physical Parameters			
m_1	$3.807\,kg$	c_1	$2.53\,Ns/m$
k_1	$11.68 * 10^3\,N/m$	m_2	$32\,g$
Δ	$15\,mm$	r	0.6
Reduced Parameters			
ε	0.84%	λ	1.43

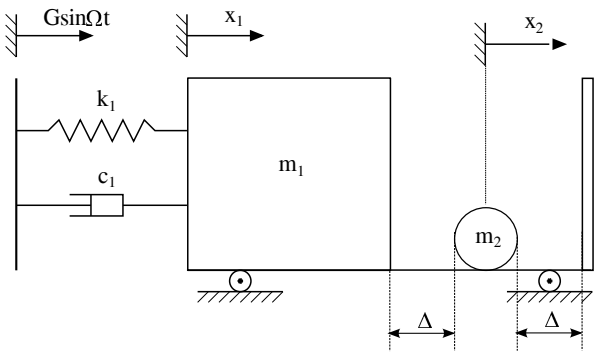

Fig. 1. Schema of the system

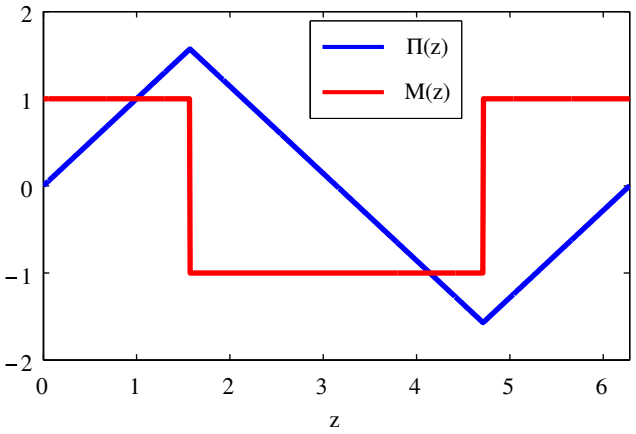

Fig. 2. Representation of the non-smooth functions $\Pi(z)$ and $M(z)$

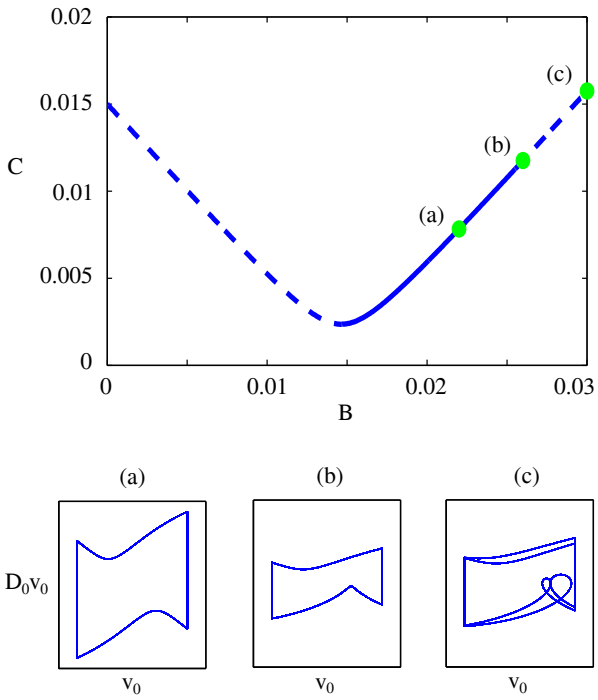

Fig. 3. SIM of the problem for $r = 0.6, \Delta = 0.015$. Straight and dotted lines denotes stable and unstable branch of the SIM respectively. Numerical phase space : (a) stable symmetric $1:1$ motion, (b) asymmetric $1:1$ motion, (c) asymmetric $2:2$ motion.

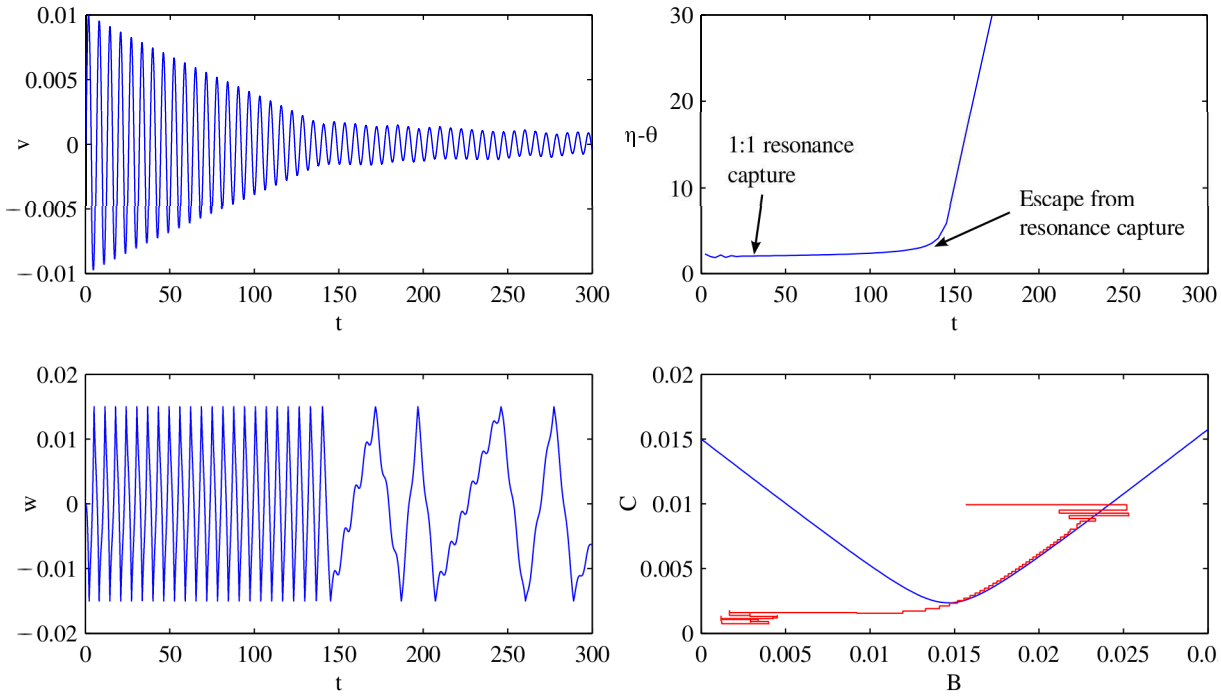

Fig. 4. Illustration of the process of TET under transient loading for $\lambda = 0.95$, $\varepsilon = 0.84\%$, $\Delta = 0.015$. (a, b) : result of numerical integration , (c) : $1:1$ resonance capture and (d) : projection of the result of numerical integration on the SIM.

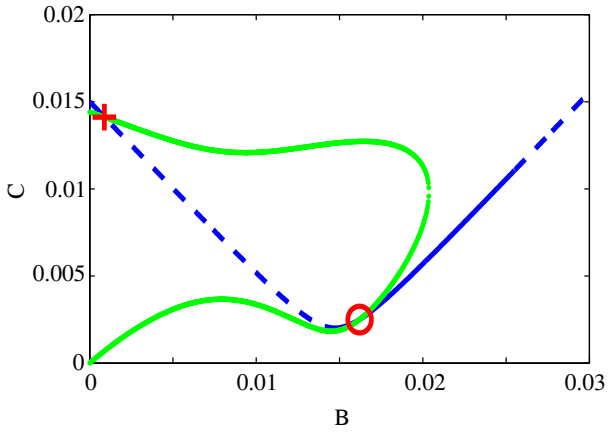

Fig. 5. Case of stable periodic response. Blue and green lines corresponds to the SIM (16) and the curves (23). Red circle (o) and red cross (+) corresponds to stable and unstable fixed points respectively. Parameters are given in Eq. (24).

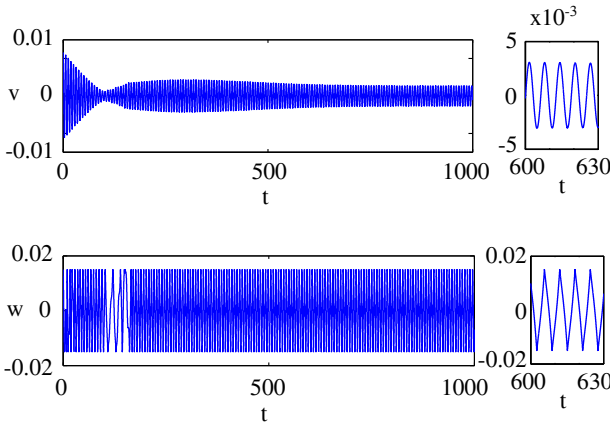

Fig. 6. Numerical integration of Eqs. (4) and (5) for the set of parameters (24) and zoom on the response

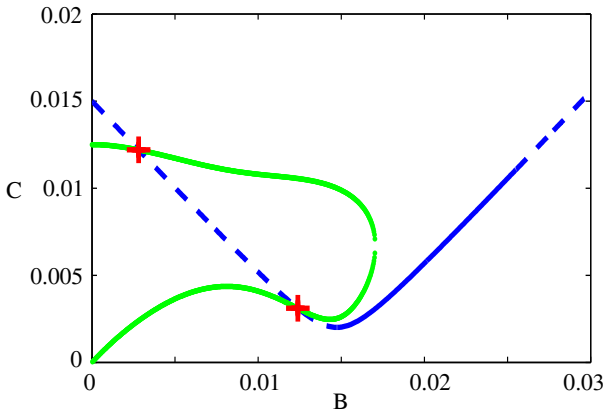

Fig. 7. Case of SMR response. Blue and green lines corresponds to the SIM (16) and the curves (23). Red cross (+) corresponds to unstable fixed points. Parameters are given in Eq. (25).

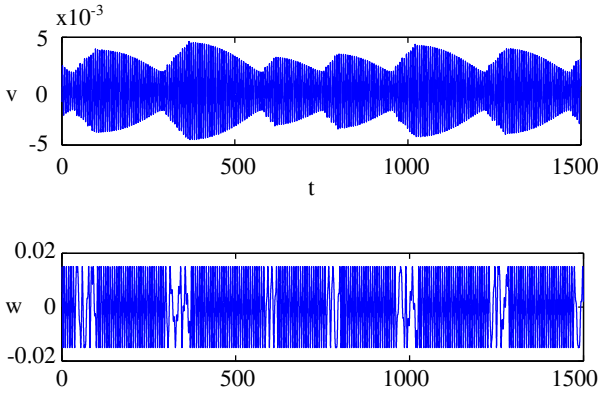

Fig. 8. Numerical integration of Eqs. (4) and (5) for the set of parameters (25).

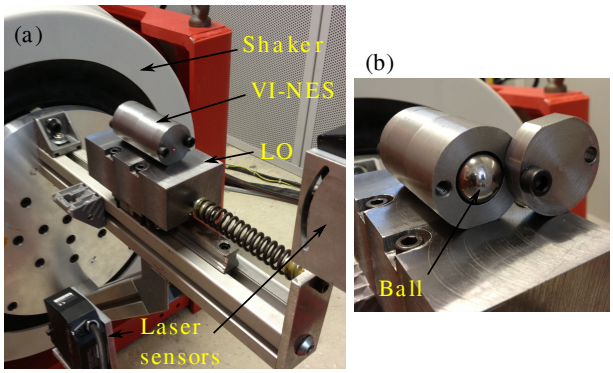

Fig. 9. Picture of the experimental setup. (a) Global view of the system, (b) detailed view of the NES.

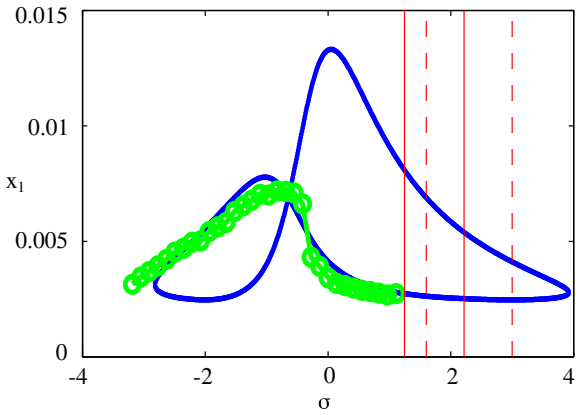

Fig. 10. Experimental and analytical frequency response curves of the LO for $G = 0.16mm$ ($A = 0.019$). Blue lines corresponds to the analytical prediction, green lines represents the experimental measurements. Straight and dashed red lines denotes the experimentally and numerically found SMR zone.

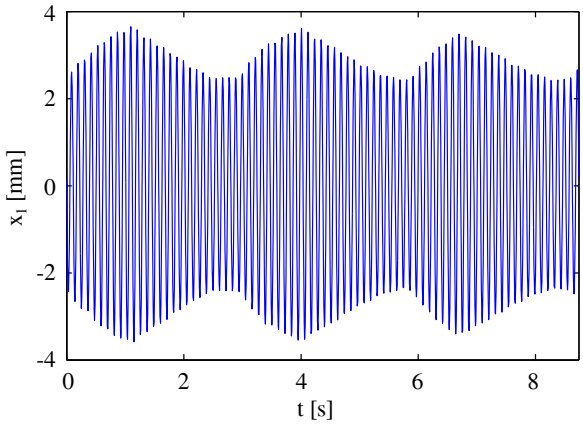

Fig. 11. Experimental measurement of SMR for $G = 0.16mm$ ($A = 0.019$) and $\sigma = 1.52$.

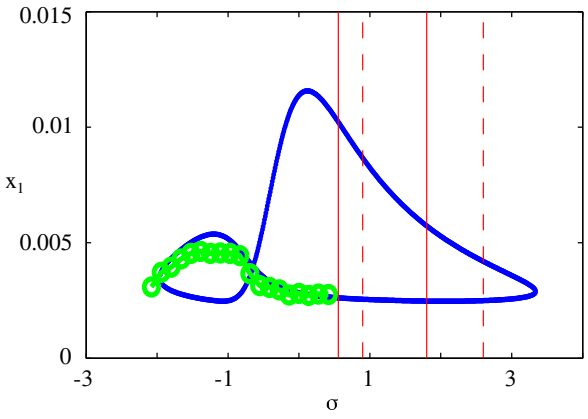

Fig. 12. Experimental and analytical frequency response curve of the LO for $G = 0.14mm$ ($A = 0.017$). Blue lines corresponds to the analytical prediction, green lines represents the experimental measurements. Straight and dashed red lines denotes the experimentally and numerically found SMR zone.

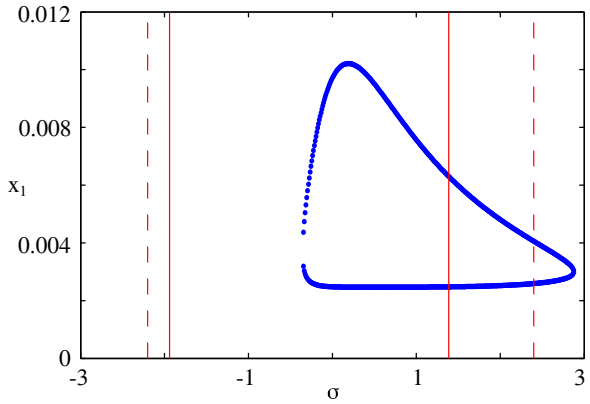

Fig. 13. Analytical frequency response curve of the LO for $G = 0.125mm$ ($A = 0.015$). Blue lines corresponds to the analytical prediction. Straight and dashed red lines denotes the experimentally and numerically found SMR zone.